Squaring the cube

Post-print of peer-reviewed article published by the Royal Society of Chemistry.
Published article available at: http://dx.doi.org/10.1039/C3DT51727F

Cite as:
Fang, M., Zhao, H., Prosvirin, A. V., Pinkowicz, D., Zhao, B., Cheng, P., Wernsdorfer, W., Brechin, E. K., & Dunbar, K. R. (2013). Squaring the cube: a family of octametallic lanthanide complexes including a Dy8 single-molecule magnet. *Dalton Transactions.*

Manuscript received: 27/06/2013; Accepted: 30/07/2013; Article published: 01/08/2013

Squaring the cube: A Family of Octametallic Lanthanide Complexes Including a Dy_8 Single-Molecule Magnet**†

Ming Fang,[1,2] Hanhua Zhao,[1] Andrey V. Prosvirin,[1] Dawid Pinkowicz,[1,3] Bin Zhao,[2,*] Peng Cheng,[2] Wolfgang Wernsdorfer,[4] Euan K. Brechin[5,*] and Kim R. Dunbar[1,*]

[1]Department of Chemistry, Texas A&M University, College Station, USA.

[2]Department of Chemistry and Key Laboratory of Advanced Energy Materials Chemistry, Ministry of Education, Nankai University, Tianjin 300071, P. R. China.

[3]Faculty of Chemistry, Jagiellonian University, Ingardena 3, 30-060 Kraków, Poland.

[4]Institut Néel, CNRS and Université Joseph Fournier, BP 166, 25 Avenue des Martyrs, 38042 Grenoble Cedex 9, France.

[5]EaStCHEM, School of Chemistry, Joseph Black Building, University of Edinburgh, West Mains Road, Edinburgh, EH9 3JJ, UK.

[*]Corresponding authors; B.Z. e-mail: zhaobin@nankai.edu.cn, E.K.B. e-mail: ebrechin@staffmail.ed.ac.uk; K.R.D. e-mail: dunbar@mail.chem.tamu.edu

[**]KRD thanks the Department of Energy (DOE-DE-FG02-02ER445999) for generous support of this research. DP gratefully acknowledges the financial support of the European Commission within the Marie Curie International Outgoing Fellowship (grant agreement no. PIOF-GA-2011-298569).

[†]Celebrating 300 years of Chemistry at The University of Edinburgh.

Supporting information:
‡Electronic Supplementary Information (ESI) available: additional structural diagrams, table with selected bond lengths and angles, additional magnetic data. CCDC 846369 (1), CCDC 846363 (2), CCDC 846362 (3), CCDC 846367 (4), CCDC 846365 (5), CCDC 846368 (6), CCDC 846366 (7), CCDC 846364 (8) contains the supplementary crystallographic data for this paper. These data can be obtained free of charge from The Cambridge Crystallographic Data Centre via www.ccdc.cam.ac.uk/data_request/cif and http://dx.doi.org/10.1039/C3DT51727F

Abstract

A series of isostructural octanuclear lanthanide complexes of general formula $[Ln_8(sao)_4(\mu_3\text{-}OH)_4(NO_3)_{12}(DMF)_{12}]$ (Ln = Nd (1), Sm (2), Eu (3), Gd (4), Tb (5), Dy (6), Ho (7), Er (8); DMF = dimethylformamide) have been prepared *via* the reactions of salicylaldoxime ($saoH_2$), tetramethylammonium hydroxide (Me_4NOH) and the appropriate lanthanide nitrate salt ($Ln(NO_3)_3{\cdot}6H_2O$). The metallic skeletons of the complexes describe $[Ln_4]$ tetrahedra encapsulated inside a $[Ln_4]$ square with the inner core stabilised through $\mu_3\text{-}OH^-$ ions and the periphery by $\mu_4\text{-}sao^{2-}$ ligands. The magnetic properties of compounds 2-8 were investigated by *dc* and *ac* magnetometry. Temperature dependent *ac* magnetic susceptibility data reveal that the dysprosium analogue (6) displays an out-of-phase signal in the absence of an applied magnetic field indicative of slow relaxation of the magnetization typical of a Single-Molecule Magnet (SMM). Micro-SQUID measurements reveal temperature and sweep rate dependent hysteresis below 1.0 K.

Introduction

The study of bistable molecular magnetic materials is a highly active research topic in the chemistry and physics communities owing, at least in part, to their promise for future applications in high density magnetic data storage and spintronic devices[1] and quantum compouting.[2] The inaugural example of single-molecule magnet (SMM) behaviour in molecular species was the mixed-valent, oxide-bridged cluster $[Mn_{12}O_{12}(O_2CCH_3)_{16}(H_2O)_4]$ (Mn_{12}-Ac) reported some 20 years ago.[3] The interplay of classical and quantum physics in Mn_{12}-Ac opened up an entirely new field of study for chemists who were tasked with the design and construction of molecules displaying analogous behaviour. This in turn provided a gateway for the discovery of fascinating new physics in zero dimensional molecules.[4]

Recently, significant attention has been directed towards the incorporation of 4*f* ions into SMMs, in both heterometallic 3*d*/4*f* and homometallic 4*f* compounds, since many lanthanide (Ln) ions possess large unquenched orbital angular momenta which imparts significant anisotropy.[5] The result that perhaps *re-focused* the attention of chemists to the suitability of employing Ln(III) (and indeed actinide) ions in the construction of SMMs was the publication of the structure and magnetic properties of the double-decker phthalocyanine (Pc) complex $[TbPc_2]$ by Ishikawa and co-workers.[6] A selection of other highlights[7] since this seminal work include, but are not limited to, a N_2^{3-} radical-bridged Tb complex exhibiting magnetic hysteresis at temperatures up to ~14 K,[4a,5b] a chemically switchable Dy-encapsulated polyoxometalate SMM,[7a] a photo-switchable Cu-Tb SMM,[7b] a Cu-Dy_3 SMM that exhibits exchange coupling of the toroidal magnetic moments,[7c] organometallic Dy(III) SMMs,[4f,7d-e] and $[Dy_5]$ pyramids that display slow magnetic relaxation up to ~40 K.[7e] We also note

that two review articles on the topic of Lanthanide-SMMs by Woodruff et al.[8a] and on the topic of Dy-based SMMs by Tang et al.[8b] were recently published.

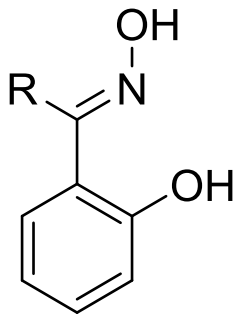

Scheme 1. Generic molecular structure of the phenolic oxime R-saoH_2. R = H, saoH_2; R = Me, Me-saoH_2, R = Et, Et-saoH_2; R = Ph, Ph-saoH_2.

Phenolic oximes (R-saoH_2; Scheme 1) have been studied for many years in transition metal (TM) coordination chemistry,[9] initially in applications relating to industrial metal extraction (particularly for Cu^{II})[10a] and anti-corrosive agents in protective coatings.[10b] In TM^{III} chemistry, the propensity of the phenolic oximes to exist in their doubly deprotonated, dianionic form (R-sao^{2-}) also renders them ideal candidates for the preparation of polymetallic SMMs, particularly in manganese chemistry.[11] However, their use in homo- and heterometallic Ln^{III} chemistry is almost completely unknown. Indeed a search of the CCDC database reveals no examples of any homometallic 4*f* cages, and only a few examples in 3*d*/4*f* chemistry:[12] a family of [Mn^{III}_6-Ln^{III}_2] hexagonal prisms,[12a,12b] heptanuclear [Mn^{III}_3-Mn^{IV}-Ln^{III}_3] (Ln = Gd, Dy) cages[12c] and 14-metallacrown-5 complexes[12d]

Herein we report the syntheses, structures and magnetic properties of a family of octanuclear Ln^{III} cages of general formula [$Ln_8(sao)_4(\mu_3\text{-}OH)_4(NO_3)_{12}(DMF)_{12}$] (Ln = Nd (**1**), Sm (**2**), Eu (**3**), Gd (**4**), Tb (**5**), Dy (**6**), Ho (**7**), Er (**8**); saoH_2 = salicylaldoxime; DMF = dimethylformamide) that represent the first examples of any homometallic Ln^{III} cages built with salicylaldoxime.

Experimental Section

Materials and Methods

Unless otherwise stated all reagents were obtained from commercial sources and were used as received without further purification. All reactions were carried out under aerobic conditions.

Elemental analyses (C, H, N) were performed by Atlantic Microlab. Variable temperature solid-state *dc* and *ac* magnetic susceptibility data from 300-1.8 K were collected on a Quantum Design MPMS-7XL SQUID magnetometer. Diamagnetic corrections were applied to the observed paramagnetic susceptibilities using Pascal's constants.[13]

Preparation of [$Ln_8(sao)_4(\mu_3\text{-}OH)_4(NO_3)_{12}(DMF)_{12}$] Ln = Nd (1), Sm (2), Eu (3), Gd (4), Tb (5), Dy (6), Ho (7), Er (8)

Separate stock solutions were prepared as follows: solution A: $Ln(NO_3)_6{\cdot}6H_2O$ (0.3 mmol), 3.0 mL of EtOH and 1.0 mL of DMF; solution B: $saoH_2$ (0.548 g, 4 mmol), $Me_4NOH{\cdot}5H_2O$ (0.724, 4 mmol) and 20 mL of EtOH. Solution A was separated into three equal portions and placed in three 6 mm O.D. Pyrex tubes and carefully layered with solution B. The tubes were sealed with Teflon tape and left to stand undisturbed. Block crystals suitable for X-ray data collection were obtained after one week, collected by filtration, washed with EtOH, and dried *in vacuo*. Elemental analyses calcd (%) for $C_{64}H_{108}N_{28}O_{60}Eu_8$ (**3**): C, 22.31; H, 3.16; N, 11.38; found: C, 22.42; H, 3.30; N, 11.30. Calcd for $C_{64}H_{108}N_{28}O_{60}Gd_8$ (**4**): C, 22.04; H, 3.12; N, 11.24; found: C, 21.27; H, 3.25; N, 10.93. Calcd for $C_{64}H_{108}N_{28}O_{60}Tb_8$ (**5**): C, 21.96; H, 3.11; N, 11.20 found: C, 22.11; H, 3.17; N, 11.16. Calcd for $C_{64}H_{108}N_{28}O_{60}Dy_8$ (**6**): C, 21.78; H, 3.08; N, 11.11; found: C, 21.48; H, 3.01; N, 11.25. Calcd for $C_{64}H_{108}N_{28}O_{60}Ho_8$ (**7**): C, 21.66; H, 3.07; N, 11.05; found: C, 21.23; H, 3.16; N, 10.90. Calcd for $C_{64}H_{108}N_{28}O_{60}Er_8$ (**8**): C, 21.54; H, 3.05; N, 10.99; found: C, 21.24; H, 3.09; N, 10.81.

Single Crystal X-ray Diffraction

Single-crystal X-ray diffraction measurements of **1**–**8** were carried out at 110 K on a Bruker APEXII X-ray diffractometer equipped with graphite-monochromated Mo$K\alpha$ radiation (λ = 0.71073 Å). Lorentz polarization and absorption corrections were applied. The structures were solved by direct methods and refined by full-matrix least-squares on F^2 (weighting scheme: $w = 1/[\sigma 2(Fo2) + (\alpha P)2 + \beta P]$, where $P = (Fo2 + 2Fc2)/3$) using the SHELXS-97 and SHELXL-97 programs.[14] All non-hydrogen atoms were refined anisotropically whereas H atoms were placed in the calculated positions and refined using the riding model. Some of the DMF molecules and nitrate anions were refined with suitable restraints to their geometries and atomic thermal parameters. Restraints of the 2θ angle were applied to the structural models of **2**, **3**, **4** and **6** to meet the completeness requirement. Crystallographic data are summarized in Table 1 with selected bond distances and angles provided in Table S1.

Results and Discussion

Single crystal X-ray diffraction reveals that all eight compounds are isostructural, crystallizing in the tetragonal space group *I-4* (Table 1). The structure of (**6**) (Ln = Dy) will be described here as a representative example of the series. The asymmetric unit is depicted in Figure S1a (see ESI) and the bond lengths are given in Table S1 (see ESI).The core of the complex (Figure 1) contains a central $[Ln^{III}_4O_4]$ cubane containing Dy1 and symmetry equivalent (s.e.) bridged by the four O-atoms derived from pyramidal μ_3-OH^- ions (O10). The peripheral metal ions (Dy2 and s.e.) themselves form a square, encapsulating the central cube. The metallic skeleton of **6** can thus be described as a tetrahedron (Dy1···Dy1', ~3.7-3.8 Å) inside a square (Dy2···Dy2, 7.7 Å), The sao^{2-} ligands exhibit the highly unusual μ_4:η^2:η^1:η^2 coordination mode (Figure S1b in ESI), with the -N9-O3- moiety of the oxime fragment bridging across one face of the $[Ln_4O_4]$ cubane, with O3 further bridging to the peripheral Dy2. The phenolic O-atom (O1) μ-bridges between Dy1 in the cube and Dy2 in the square. The remaining coordination sites on Dy1 are filled with two terminally bonded DMF molecules, and on Dy2 by three chelating NO_3^- ions and one DMF. Dy1 is eight-coordinate and distorted square-antiprismatic in geometry with a $[O_7N]$ coordination sphere. Dy2 is nine-coordinate with a $[O_9]$ coordination sphere. There is one intramolecular H-bond between the OH^- group and the nitrate anion with OH···O distance of 1.998 Å stabilizing the core of the molecule. There are no significant intermolecular contacts (no H-bonds or π-π stacking). The closest intermolecular distances are between the C-H groups of the phenyl rings (C-H···H-C distance of 2.359). In all compounds **1-8** the Ln−O and Ln−N distances are in the 2.3−2.6 Å range typical for Ln complexes. The Ln···Ln distances within the Ln_8 core are around 4.0 Å (see Table S1), the closest distances between two Ln atoms of the adjacent Ln_8 molecules is around 10 Å.

(turn to next page →)

Compound	**1** **Ln = Nd**	**2** **Ln = Sm**	**3** **Ln = Eu**	**4** **Ln = Gd**
Formula	$C_{64}H_{108}N_{28}Ln_8O_{60}$			
FW [g·mol^{-1}]	3383.70	3432.66	3445.46	3487.78
Crystal system	tetragonal			
Space group	*I -4*			
Unit cell [Å]				
a	18.261(3)	18.150(2)	18.111(3)	18.146(5)
c	19.135(4)	19.137(5)	19.188(4)	19.246(9)
V [Å^3]	6381(2)	6304(2)	6294(2)	6337(4)
Z	2	2	2	2
d_{calcd} [g·cm^{-3}]	1.761	1.808	1.818	1.828
Abs. coeff. [mm^{-1}]	3.288	3.760	4.020	4.220
Max transmission	0.460	0.551	0.379	0.543
Min transmission	0.419	0.322	0.326	0.444
F(000)	3296.0	3328.0	3344.0	3360.0
Completeness θ [%]	99.9	100	100	100
Data	7091	5543	5527	5587
Restraints	245	300	300	119
Parameters	367	367	367	367
GooF	1.080	1.077	1.086	1.144
R_1	0.0445	0.0442	0.0444	0.0372
wR_2	0.1279	0.1252	0.1251	0.1055
Largest diff. peak	1.390	1.417	1.714	1.672
Largest diff. hole	-1.289	-1.257	-1.234	-1.315
Compound	**5** Ln = Tb	**6** Ln = Dy	**7** Ln = Ho	**8** Ln = Er
Formula	$C_{64}H_{108}N_{28}Ln_8O_{60}$			
FW [g·mol^{-1}]	3501.14	3529.78	3549.22	3567.86
Crystal system	tetragonal			
Space group	*I -4*			
Unit cell [Å]				
a	18.022(4)	17.999(7)	17.970(1)	17.939(3)
c	19.143(7)	19.209(2)	19.184(2)	19.245(4)
V [Å^3]	6218(3)	6223(6)	6195(1)	6194(2)
Z	2	2	2	2
d_{calcd} [g·cm^{-3}]	1.870	1.884	1.903	1.913
Abs. coeff. [mm^{-1}]	4.584	4.837	5.143	5.454
Max transmission	0.382	0.325	0.308	0.367
Min transmission	0.340	0.325	0.290	0.244
F(000)	3376.0	3392.0	3408.0	3424.0
Completeness θ [%]	99.6	100	95.4	99.0
Data	4636	5482	4315	4505
Restraints	66	336	101	228
Parameters	367	367	367	367
GooF	1.127	1.237	1.069	1.099
R_1	0.0347	0.0396	0.0421	0.0559
wR_2	0.0979	0.1039	0.1218	0.1530
Largest diff. peak	1.446	1.560	1.655	2.054
Largest diff. hole	-0.702	-1.410	-1.058	-2.239

Table 1. Selected crystallographic parameters and data for 1 – 8.

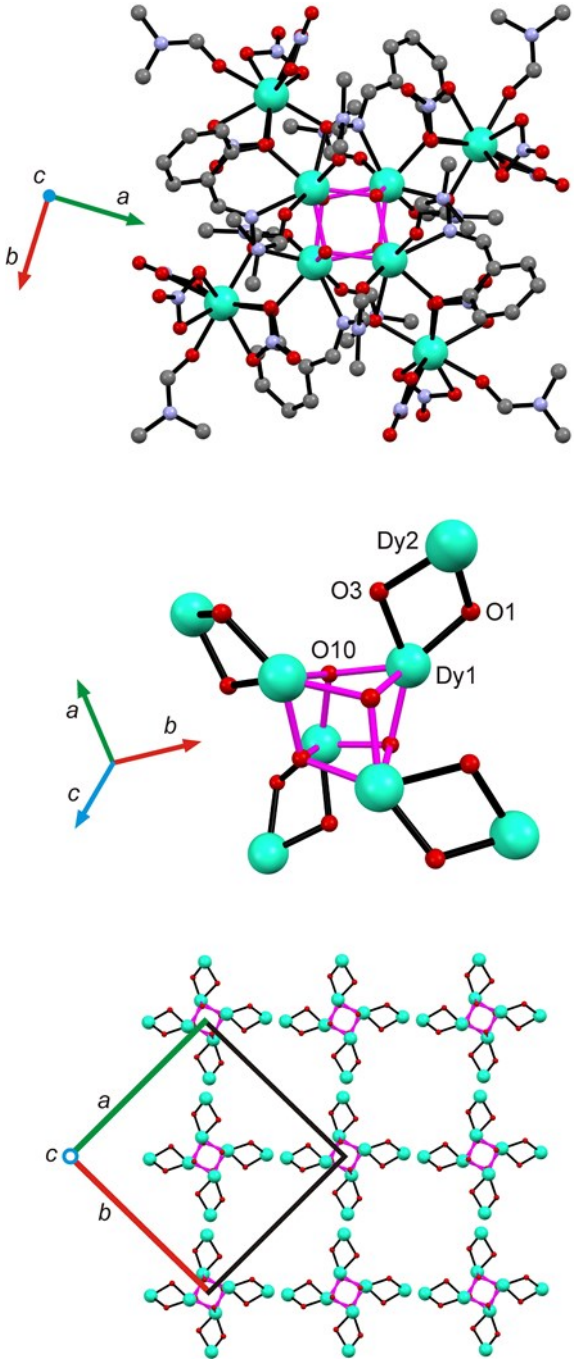

Figure 1. Molecular structure of **6** (top), the Dy_8 core (middle) and the structural diagram showing the arrangement of the Dy_8 cores in the unit cell (bottom). Dy - cyan; O - red; N - blue, C – grey, H – omitted for clarity. The solid pink lines highlight the central $\{Dy_4O_4\}$ cubane unit.

The cage molecules pack in superimposable rows in all three unit cell directions, affording the aesthetically pleasing brickwork-like topology shown in Figure S1a (see ESI). It is worth mentioning that in all eight crystal structures there are solvent accessible voids between the cages (ca. 4.2 % of the total volume) that seem to be intrinsic to this family of compounds.

Interestingly, the structure of **6** is somewhat similar to the octanuclear Fe^{III} complex $[Fe_8O_4(sao)_8(py)_4]$ whose metallic skeleton describes a cube encapsulated inside a tetrahedron.[15] In the literature there are also several examples of Ln^{III}_8 cage compounds.[16] All of them, however, exhibit completely different topologies. A common motif is the assembly of two tetranuclear Dy^{III}_4 units.[16a-16c] Tang et al. reported Dy^{III}_8 molecule with a tub-shaped metallic core[16d] and Colacio et al. reported a family of 16-membered Ln_8 macrocycles.[16e]

Magnetic Properties

Variable-temperature *dc* magnetic susceptibility data for compounds **2-8** were collected on powdered microcrystalline samples over the temperature range 1.8−300 K and under an applied field of 1000 Oe (Figure 2 and Figure 3). The magnetic properties of **4** are discussed first since the isotropifc f^7 Gd^{III} ion has no orbital contribution. The $\chi_M T$ product of **4** at 300 K (61.06 $cm^3 \cdot K \cdot mol^{-1}$) is consistent with the spin only value of 63.00 $cm^3 \cdot K \cdot mol^{-1}$ expected for eight non-interacting Gd^{III} ions ($S = 7/2$, $L = 0$, $^8S_{7/2}$, $g = 2$: $C = 7.875$ $cm^3 \cdot K \cdot mol^{-1}$).[17] As temperature is decreased $\chi_M T$ remains relatively constant, and at 30 K is 57.73 $cm^3 \cdot K \cdot mol^{-1}$. Below 14 K the $\chi_M T$ dependence exhibits a sharp decrease reaching a value 32.07 $cm^3 \cdot K \cdot mol^{-1}$ at 2 K. This behaviour is indicative of the presence of very weak antiferromagnetic interactions between the Gd^{III} ions within the Gd_8 cage. Compounds **2** and **3** and **5-8** exhibit very different magnetic behaviour than that of **4**, likely due to the significant orbital contributions of their respective Ln(III) ions. Due to the existence of inter-electronic repulsion and spin-orbit coupling, the $4f^n$ configuration is split into $^{2S+1}L_J$ states. Moreover, influenced by the weak crystal field perturbation, each of these states can be further split into m_J sublevels which are thermally populated at room temperature. Progressive thermal depopulation of these sublevels leads to a $\chi_M T$ response that decreases as the temperature is lowered owing to Boltzmann depopulation of the excited states.

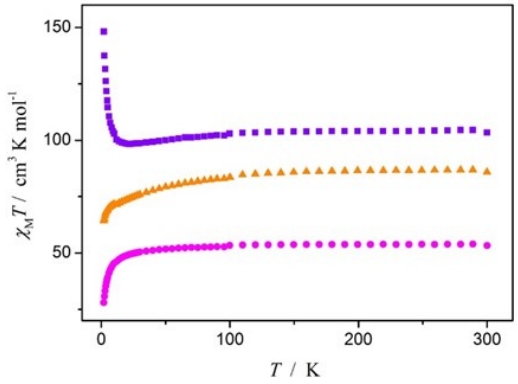

Figure 2. Plots of $\chi_M T$ vs. T for **4** (magenta ●), **5** (orange ▲) and **6** (violet ■) under an applied magnetic field of 1000 Oe.

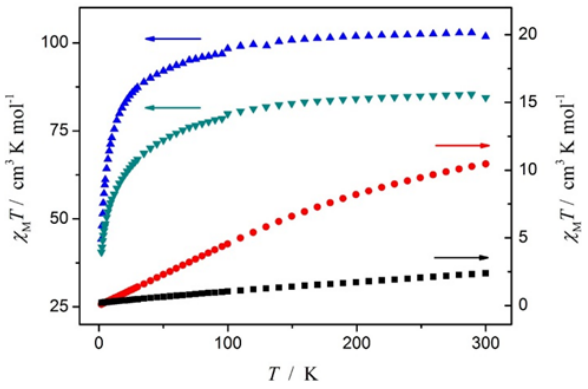

Figure 3. Plots of $\chi_M T$ vs. T for **2** (black ■), **3** (red ●), **7** (blue ▲) and **8** (cyan ▼) under an applied magnetic field of 1000 Oe.

For **2**, the value of $\chi_M T$ at 300 K is 2.39 $cm^3 \cdot K \cdot mol^{-1}$, much higher than the theoretical value of 0.72 $cm^3 \cdot K \cdot mol^{-1}$ expected for eight independent Sm(III) ions ($S = 5/2$, $L = 5$, $^6H_{5/2}$, $g = 2/7$: $C = 0.09$ $cm^3 \cdot K \cdot mol^{-1}$).[17] The large experimental $\chi_M T$ value of **2** at room temperature is attributed to the population of excited states such as $^6H_{7/2}$.[18] The $\chi_M T$ dependence of **2** decreases with decreasing temperature and reaches 0.19 $cm^3 \cdot K \cdot mol^{-1}$ at 2 K, reflecting both the deopoulation of said excited states and possible weak antiferromagnetic interactions between neighbouring metal ions. For compound **3**, $\chi_M T$ is 11.56 $cm^3 \cdot K \cdot mol^{-1}$ at room temperature (Figure 3) and in view of the non-magnetic $^7F_0$ ground state of Eu(III), this discrepancy is attributed to non-negligible thermal population of excited states such as $^7F_1$ and $^7F_2$.[18] $\chi_M T$ then decreases with decreasing temperature and at 1.8 K approaches 0.10 $cm^3 \cdot K \cdot mol^{-1}$ simply reflecting the depopulation of the paramagnetic excited states and as expected for a Eu(III)ion with a non-magnetic ground state.

In case of compounds **5**, **7**, and **8**, the observed $\chi_M T$ values at room temperature are 93.91, 110.06 and 91.23 $cm^3 \cdot K \cdot mol^{-1}$, respectively (Figure 2 and 3). These values are close to the corresponding theoretical values of 94.56, 112.56 and 91.58 $cm^3 \cdot K \cdot mol^{-1}$ expected for eight non-interacting Tb(III) ions ($S = 3$, $L = 3$, $^7F_6$, $g = 3/2$: $C =$ $cm^3 \cdot K \cdot mol^{-1}$) for **5**, eight non-interacting Ho(III) ions ($S = 2$, $L = 6$, $^5I_8$, $g = 5/4$: $C = 14.07$ $cm^3 \cdot K \cdot mol^{-1}$) for **7**, and eight non-interacting Er(III) ions ($S = 3/2$, $L = 6$, $^4I_{15/2}$, $g = 6/5$: $C = 11.48$ $cm^3 \cdot K \cdot mol^{-1}$), respectively.[17] At lower temperatures, the thermal variations of $\chi_M T$ for **5**, **7** and **8** undergo a decrease to reach 70.19, 47.83 and 43.81 $cm^3 \cdot K \cdot mol^{-1}$ at 2 K, respectively. Finally, measurements on **6** reveal that the $\chi_M T$ value at room temperature is 109.74 $cm^3 \cdot K \cdot mol^{-1}$ (Figure 2), which is close to the theoretical value of 113.36 $cm^3 \cdot K \cdot mol^{-1}$ expected for eight non-interacting Dy(III) ions ($S = 5/2$, $L = 5$, $^6H_{15/2}$, $g = 4/3$: $C = 14.17$ cm^3 K mol^{-1}).[17] Upon cooling, the $\chi_M T$ product decreases gradually to reach 104.47 $cm^3 \cdot K \cdot mol^{-1}$ at 22 K and then abruptly increases and reaches a maximum value of 157.22 $cm^3 \cdot K \cdot mol^{-1}$ at 2 K this may indicate the presence of significant ferromagnetic interactions within the Dy_8 core of the molecule.

The field dependence of the magnetization of compounds **4**–**6** was measured at T = 1.8 K in fields from 0-70 kOe (Figure 4). In each case the increase of the magnetization is quite steep reaching 55.88, 39.70 and 47.37 $N\beta$ at 70 kOe for **4**, **5** and **6**, respectively. In case of compound **6** the magnetization reaches the value close to the maximum at fields as low as 7000 Oe which further confirms the ferromagnetic character of the interactions between Dy atoms. The values at 70 kOe for **5** and **6** are much lower than the expected saturation value of 72 $N\beta$ and 80 $N\beta$ for eight non- interacting Tb(III) and Dy(III) ions, respectively. This behaviour indicates the presence of significant magnetic anisotropy and/or the lack of a well-defined ground state.

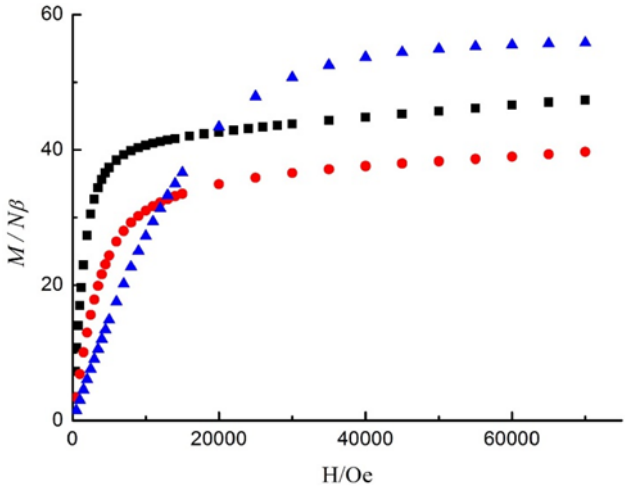

Figure 4. The field dependence of the magnetization for compounds **4**-**6** measured at 1.8 K (**4** – blue ▲, **5** – red ●, **6** – black ■).

In order to probe the magnetization dynamics of the new compounds, the temperature and frequency dependence of the *ac* magnetic susceptibilities were performed in the absence of an applied *dc* magnetic field; however only compound **6** (Dy_8) exhibits a frequency dependence under these conditions. Figure 5 depicts the temperature dependence of the in-phase (plotted as $\chi_M'T$) and the out-of-phase ($\chi_{M''}$) component of the *ac* magnetic susceptibility under zero *dc* magnetic field, measured at six different frequencies in the 1.8–9 K temperature range. The response clearly indicates slow relaxation of the magnetization in **6**. As shown in Figure 6, *ac* susceptibility data collected in the absence of an external *dc* magnetic field display temperature-dependent peaks in the χ_M'' versus ν (ν = *ac* field frequency) plot. This finding further confirms the slow relaxation of the magnetization in **6**. The frequency values at which the maximum of the $\chi''(\nu)$ dependence occurs were used to plot the T^{-1} *vs*. $\ln(2\pi\nu)$ which obeys the Arrhenius law $T^{-1} = -k_B/\Delta E \cdot \{\ln(2\pi\nu) + \ln(\tau_0)\}$ (Figure7). The best linear fit of the T^{-1} vs. $\ln(2\pi\nu)$ dependence yields the energy barrier for the magnetization reversal for

compound **6** $\Delta E/k_B$ = 6.17 K and $\tau_0 = 3.11\times10^{-5}$ s. The value of the pre-exponential factor deviates from the typical ~10^{-9} s because the slow magnetic relaxation in **6**, in the investigated temperature range, is probably controlled by the quantum tunnelling process.

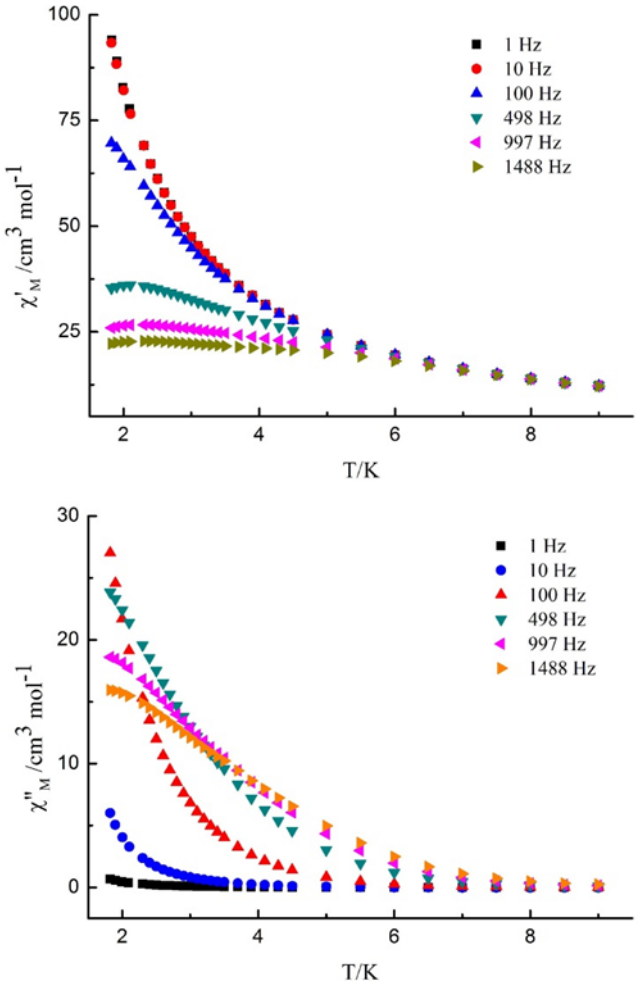

← ***Figure 5.*** Temperature dependence of the in-phase (top) and out-of-phase (bottom) ac magnetic susceptibility for 6 measured at six different frequencies (H_{ac} = 5 Oe, H_{dc}= 0 Oe).

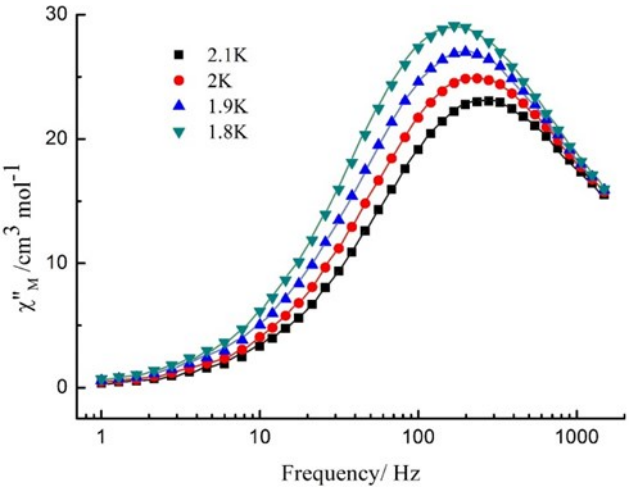

Figure 6. → Frequency dependence of the out-of-phase (χ'') *ac* susceptibility for **6** in H_{dc}= 0 Oe at the indicated temperatures (solid lines are a guide for the eye).

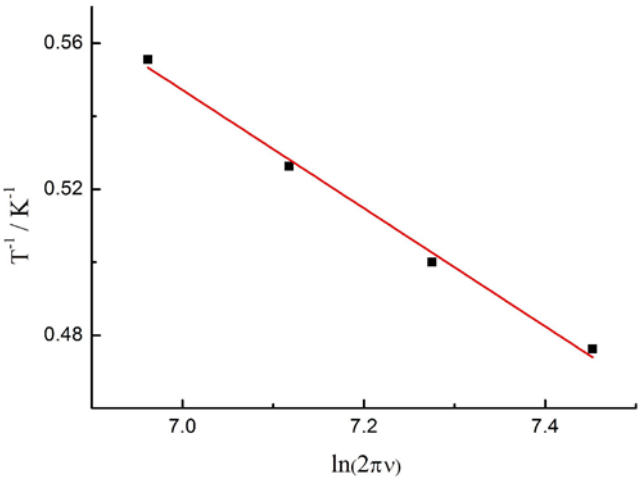

Figure 7. The least-squares fit of the experimental data to the Arrhenius equation for **6** at H_{dc}= 0 Oe. The energy barrier $\Delta E/k_B$ = 6.17 K and the pre-exponential factor $\tau_0 = 3.11\times10^{-5}$ s.

A generalized Debye model[19] was used to fit the Cole-Cole plot for **6** (Figure 8) in the temperature range 1.8-2.1 K:

$$\chi(\omega) = \chi_S + \frac{\chi_T - \chi_S}{1+(i\omega\tau)^{1-\alpha}} (1)$$

The parameter α was found to be almost constant at 0.2 (see Table S2 in the ESI for details). The best linear fit of the T^{-1} vs. ln(τ) dependence yields $\Delta E/k_B$ = 5.1 K and $\tau_0 = 4.73\times10^{-5}$ s, consistent with the values obtained from the frequency maxima of the χ'' vs. ν plot.

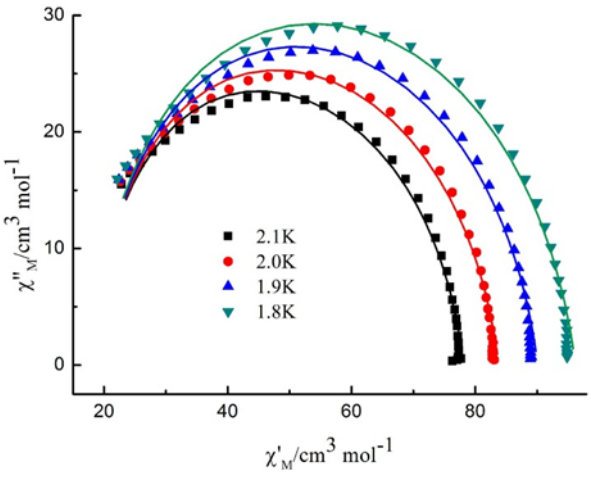

Figure 8. The Cole-Cole plot for complex **6** at different temperatures (H_{dc} = 0 Oe). The solid lines represent the best fit to the Debye model of Eq. (1). See text for details.

The slow relaxation of magnetization of **6** was also studied by means of micro-SQUID *dc* magnetmetry.[20] Hysteresis loops were collected with the field applied along the easy-axis of an oriented single crystal in the 0.03-1.0 K temperature range. Below 1.0 K at a 0.07 T/s magnetic field sweep rate, hysteretic behaviour was observed which confirms that **6** is indeed an SMM (Figure 9; at 30 mK and 0.07 T/s the observed coercive field H_c = 0.1 T). The observed coercivity is strongly temperature and sweep-rate dependent (Figure S1 in the ESI) as expected for SMMs.[19] Similar open hysteresis loops were observed before for example in Dy_3Cu_6 molecule reported by Aronica et al.[21]

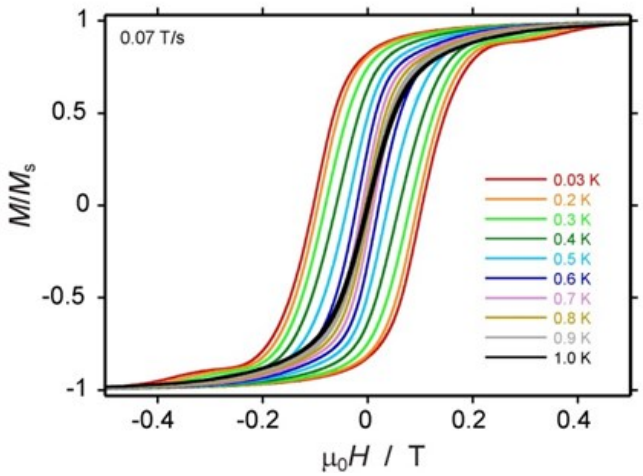

Figure 9. Micro-SQUID magnetization scans collected in the 0.03-1.0 K temperature range for complex **6** at 0.07 T/s. The magnetization value is normalized to the magnetization value at 0.5 T.

The hysteresis loops recorded below 0.3 K and at a sweep rate 0.07 T/s reveal a step-like feature at ~0.4 T due to resonant quantum tunnelling. Remarkably, no quantum tunnelling relaxation step at zero magnetic field has been observed. This is in agreement with the frequency dependence of the *ac* magnetic susceptibility at H_{dc} = 0 Oe. The lack of the fast zero-field relaxation might be due to the intramolecular ferromagnetic interactions between Dy centers within the Dy_8 core of the molecule.[21] *Dc* magnetization decay measurements were performed in order to assess the relaxation times in the subkelvin temperature range (Figure 10 inset). The plot of the temperature dependence of the relaxation times ln(τ) vs. T^{-1} obeys the Arrhenius law $\tau = \tau_0 \exp(\Delta E/kT)$ in the high temperature range (0.8 – 0.5 K) and is consistent with the results obtained from the *ac* data at 1.8-2.1 K (Figure 10).

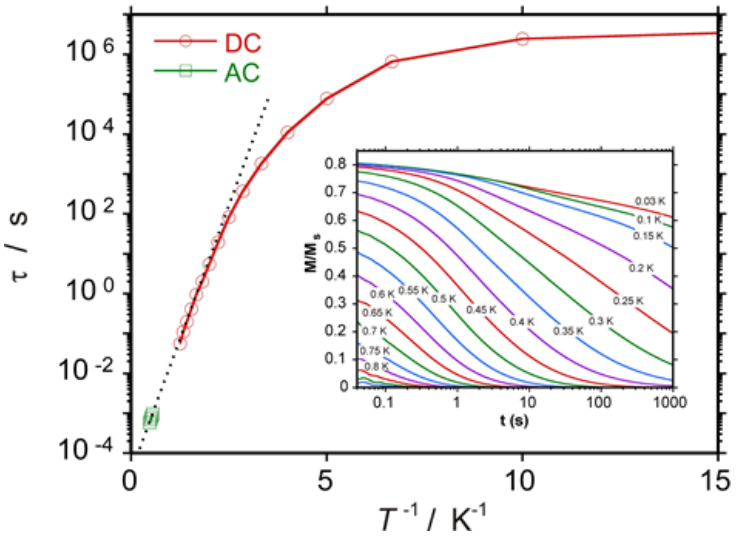

Figure 10. Arrhnius plot of the AC (green squares) and DC (red circles) relaxation times versus the inverse of the temperature. Inset: micro-SQUID magnetization decay at zero applied field and the indicated temperatures.

To further study the magnetic relaxation behaviour of **6** and to check for quantum tunneling effects, the frequency dependence of the *ac* susceptibility in the 1.8 – 2.2 K range was measured with applied *dc* fields of 1, 2, 3 and 4 kOe (Figures S2-S5 in the ESI). The peaks observed at zero field at ~200 Hz in the χ_M'' *vs.* ν plots shift towards higher frequencies when an external magnetic field is applied (to *ca.* 400 Hz at 1 kOe and 900 Hz at 2 kOe). Above 3 kOe, the high-frequency peak nearly disappears and the tail of a new peak at lower frequencies appears (~ 1Hz). Fitting the 1 kOe data to the Arrhenius law gives an energy barrier $\Delta E/k_B$ of 7.2 K, which is only slightly higher than the value obtained at zero field (6.2 K). The pre-exponential factor τ_0 at 1 kOe is 9.03×10^{-5} s which is also only slightly higher than that obtained under zero field. lWe note that two relaxation processes can be clearly seen under the influence of an applied field, as evidenced in the Cole-Cole plots of Figures S2-S5. Multiple relaxation processes have been previously reported for other Dy(III) SMMs.[22] Fitting Cole-Cole plots under external magnetic fields above 1 kOe was not possible due to insufficient data caused by the instrument limitations (frequency range 0.1 – 1500 Hz). Further studies under applied magnetic fields over a wider frequency range 0.1 – 10 kHz are necessary to fully understand the nature of the magnetic relaxation in **6**.

Conclusions

A systematic study of eight octanuclear lanthanide cage compounds of the type $[Ln_8(sao)_4(\mu_3\text{-}OH)_4(NO_3)_{12}(DMF)_{12}]$ was undertaken. The isostructural compounds crystallize in the tetragonal

system, space group *I-4* and describe a [Ln_4] tetrahedron encapsulated inside a larger [Ln_4] square. Magnetic measurements reveal that only the Dy^{III} analogue exhibits SMM behaviour, and does so even in the absence of an applied magnetic field. This is quite rare for homometallic Ln SMM in which rapid QTM at $H = 0$ negates the observation of hysteresis in magnetization versus field studies. Complex **6** is one of the very few examples[4a, 23] of multinuclear homometallic Ln SMM to exhibit such hysteresis and slow magnetic relaxation at zero applied *dc* field. The observation of clear hysteresis in **6** at $T = 1.0$ K therefore highlights a potential design principle for constructing novel Ln-based SMMs: the decoration of the peripheral ligand sheath with H-bond donor/acceptor moieties (or equivalent) that will encourage the formation of weak intermolecular interactions, switching off zero-field tunnelling.

Notes and references

[1] a) D. Gatteschi, R. Sessoli and J. Villain, *Molecular Nanomagnets*, 2006; b) L. Bogani and W. Wernsdorfer, *Nature Mater.*, 2008, **7**, 179; c) M. Mannini, F. Pineider, P. Sainctavit, C. Danieli, E. Otero, C. Sciancalepore, A. M. Talarico, M.-A. Arrio, A. Cornia, D. Gatteschi and R. Sessoli, *Nature Mater*., 2009, **8**, 194.

[2] a) M. N. Leuenberger, D. Loss, *Nature*, 2001, **410**, 789; c) J. Lehmann, A. Gaita-Arino, E. Coronado and D. Loss *Nature Nanotech.*, 2007, **2**, 312; c) M. Ganzhorn, S. Klyatskaya, M. Ruben, W. Wernsdorfer, *Nature. Nanotech.*, 2013, **8**, 165

[3] R. Sessoli, D. Gatteschi, A. Caneschi and M. A. Novak *Nature*, 1993, **365**, 141

[4] For *some of the most recent examples of polynuclear Ln SMMs see*: a) J. D. Rinehart, M. Fang, W. J. Evans and J. R. Long, *Nat. Chem.* 2011, **3**, 538; b) K. S. Pedersen, J. Dreiser, J. Nehrkorn, M. Gysler, M. Schau-Magnussen, A. Schnegg, K. Holldack, R. Bittl, S. Piligkos, H. Weihe, P. Tregenna-Piggott, O. Waldmann and J. Bendix, *Chem. Commun.*, 2011, **47**, 6918; c) E. J. Shelter, F. Karadas, C. Avendano, A. V. Prosvirin, W. Wernsdorfer and K. R. Dunbar *J. Am. Chem. Soc.*, 2007, **129**, 8139; d) K. J. Heroux, H. M. Quddusi, J. Liu, J. R. O'Brien, M. Nakano, E. del Barco, S. Hill and D. N. Hendrickson, *Inorg. Chem.*, 2011, **50**, 7367. *Examples of mononuclear lanthanide-based SMMs*: e) M.-E. Boulon, G. Cucinotta, J. Luzon, C. Degl'Innocenti, M. Perfetti, K. Bernot, G. Calvez, A. Caneschi and R. Sessoli, *Angew. Chem. Int. Ed.,* 2013, **52**, 350; f) M. Jeletic, P.-H. Lin, J. J. Le Roy, I. Korobkov, S. I. Gorelsky and M. Murugesu, *J. Am. Chem. Soc.,* 2011, **133**, 19286. For *examples of mononuclear transition metal SMMs or "SIMs" see*: g) J. Vallejo, I. Castro, R. Ruiz-Garcia, J. Cano, M. Julve, F. Lloret, G. De Munno, W. Wernsdorfer and E. Pardo, *J. Am. Chem. Soc.* 2012, **134**, 15704; h) J. M. Zadrozny, M. Atanasov, A. M. Bryan, C.-Y. Lin, B. D. Rekken, P. P. Power, F. Neese and J. R. Long, *Chem. Sci.* 2013, **4**, 125; i) Y.-Y. Zhu, C. Cui, Y. Q. Zhang, J.-H. Jia, X. Guo, C. Gao, K. Qian, S.-D. Jiang, B.-W. Wang, Z.-M. Wang and S. Gao, *Chem. Sci.,* 2013, **4**, 1802.

[5] a) J. D. Rinehart, J. R. Long *Chem. Sci.* 2011, **2**, 2078; b) J. D. Rinehart, M. Fang, W. J. Evans and J. R. Long, *J. Am. Chem. Soc.* 2011, **133**, 14236; c) S. Demir, J. M. Zadrozny, M. Nippe and J. R. Long, *J. Am. Chem. Soc*., 2012, **134**, 18456; d) C. Benelli, A. Caneschi, D. Gatteschi, O. Guillou, L. Pardi, P. Rey *Inorg. Chim. Acta*, 1989, **160**, 1; e) C. Benelli, A. Caneschi, D. Gatteschi, O. Guillou, L. Pardi, *Inorg. Chem.* 1990, **29**, 1750

[6] N. Ishikawa, M. Sugita, T. Ishikawa, S. Koshihara and Y. Kaizu *J. Am. Chem. Soc,*. 2003, **125**, 8694.

[7] a) K. Suzuki, R. Sato and N. Mizuno, *Chem. Sci.* 2013, **4**, 596; b) T. Shiga, H. Miyasaka, M. Yamashita, M. Morimoto and M. Irie *Dalton. Trans.,* 2011, **40**, 2275; c) G. Novitchi, G. Pilet, L. Ungur, V. V. Moshchalkov, W. Wernsdorfer, L. F. Chibotaru, D. Luneau and A. K. Powell, *Chem. Sci.,* 2012, **3**, 1169; d) A. Venugopal, F. Tuna, T. P. Spaniol, L. Ungur, L. F. Chibotaru, J. Okuda and R. A. Layfield, *Chem. Commun*., 2013, **49**, 901; e) S. A. Sulway, R. A. Layfield, F. Tuna, W. Wernsdorfer and R. E. P. Winpenny, *Chem. Commun*., 2012, **48**, 1508; f) R. J. Blagg, C. A. Muryn, E. J. L. McInnes, F. Tuna and R. E. P. Winpenny, *Angew. Chem. Int. Ed.,* 2011, **50**, 6530.

[8] a) D. N. Woodruff, R. E. P. Winpenny, R. A. Layfield *Chem. Rev.* 2013, DOI: 10.1021/cr400018q; b) P. Zhang, Y.-N. Guo and J. Tang, *Coord. Chem. Rev.* 2013, **257**, 1728.

[9] a) A. G. Smith, P. A. Tasker, D. J. White, *Coord. Chem. Rev.* 2003, **241**, 61; b) P. Chaudhuri, *Coord. Chem. Rev.*, 2003, **243**, 143.

[10] a) G. A. Kordosky, K. C. Sole, P. M. Cole, J. S. Preston and D. A. Robinson (Eds.), *Proceedings of the International Solvent Extraction Conference,* South African Institute of Mining and Metallurgy, Johannesburg, 2002, 853; b) J. M. Thorpe, R. L. Beddoes, D. Collison, C. D. Garner, M. Helliwell, J. M. Holmes and P. A. Tasker *Angew. Chem. Int. Ed.,* 1999, **38**, 1119.

[11] *See for example:* a) E. Houton, S. M. Taylor, C. C. Beedle, J. Cano, S. Piligkos, S. Hill, A. G. Ryder, E. K. Brechin and L. F. Jones, *Dalton Trans*., 2012, **41**, 8340; b) R. Inglis, C. J. Milios, L. F. Jones, S. Piligkos and E. K. Brechin, *Chem. Commun*., 2012, **48**, 181; c) R. Inglis, E. Houton, J. Liu, A. Prescimone, J. Cano, S. Piligkos, S. Hill, L. F. Jones and E.K. Brechin, *Dalton Trans*., 2011, **40**, 9999; d) R. Inglis, S. M. Taylor, L. F. Jones, G. S. Papaefstathiou, S. P. Perlepes, S. Datta, S. Hill, W.Wernsdorfer and E. K. Brechin, *Dalton Trans*., 2009, **0**, 9157; e) R. Inglis, L. F. Jones, C. J. Milios, S. Datta, A. Collins, S. Parsons, W. Wernsdorfer, S. Hill, S. P. Perlepes, S. Piligkos and E. K. Brechin, *Dalton Trans*., 2009, **0**, 3403; f) R. Inglis, L. F. Jones, G. Karotsis, A. Collins, S. Parsons, S. P. Perlepes, W.Wernsdorfer and Euan K. Brechin, *Chem. Commun*., 2008, 5924; g) C. J. Milios, S. Piligkos and E. K. Brechin, *Dalton Trans*., 2008, 1809; h) C. J. Milios, R. Inglis, A. Vinslava, R. Bagai, W. Wernsdorfer, S. Parsons, S. P. Perlepes, G. Christou and E. K. Brechin, *J. Am. Chem. Soc.,* 2007, **129**, 12505; i) C. J. Milios, C. P. Raptopoulou, A. Terzis, F. Lloret, R. Vicente, S. P. Perlepes and A. Escuer, *Angew. Chem. Int. Ed*., 2004, **43**, 212.

[12] a) G. Rigaux, R. Inglis, S. Morrison, A. Prescimone, C. Cadiou, M. Evangelisti and E. K. Brechin, *Dalton Trans*., 2011, **40**, 4797; b) M. Hołyńska, D. Premužić, I.-R. Jeon, W. Wernsdorfer, R. Clérac and S. Dehnen, *Chem. Eur. J.,* 2011, **17**, 9605; c) C.-M. Liu, D.-Q. Zhang, D.-B. Zhu *Dalton Trans.* 2010, **39**, 11325-11328; d) T. T. Boron III, J. W. Kampf, V. L. Pecoraro *Inorg. Chem.* 2010, **49**, 9104-9106

[13] G. A. Bain and J. F. Berry *J. Chem. Educ.* 2008, **85**, 532

[14] G. M. Sheldrick, *Acta Cryst.* 2008, **A64**, 112-122

[15] I. A. Gass, C. J. Milios, A. G. Whittaker, F. P. A. Fabiani, S. Parsons, M. Murrie, S. P. Perlepes, E. K. Brechin *Inorg. Chem.* 2006, **45**, 5281-5283

[16] a) J. L. Bris, L. G. Hubert Pfalzgraf, M. Rolland, Y. Garcia *Inorg. Chem. Commun.* 2006, **9**, 695-698; b) H. Ke, P. Gamez, L. Zhao, G.-F. Xu, S. Xue, J. Tang *Inorg. Chem.* 2010, **49**, 7549-7557; c) Y.-L. Miao, J.-L. Liu, J.-Y. Li, J.-D. Leng, Y.-C. Ou, M.-L. Tong *Dalton Trans.* 2011, **40**, 10229-10236; d) Y.-N. Guo, X.-H. Chen, S. Xue, J. Tang *Inorg. Chem.* 2012, **51**, 4035-4042; e) V. Chandrasekhar, P. Bag, E. Colacio *Inorg. Chem.* 2013, **52**, 4562-4570.

[17] C. Benelli and D. Gatteschi, *Chem. Rev.* 2002, **102**, 2369

[18] M. Andruh, E. Bakalbassis, O. Kahn, J. C. Trombe and P. Porcher *Inorg. Chem.,* 1993, **32**, 1616

[19] D. Gatteschi, R. Sessoli and J. Villain, *Molecular Nanomagnets*, Oxford University Press, New York, 2006.

[20] W. Wernsdorfer, *Adv. Chem. Phys.* 2001, **118**, 99.

[21] C. Aronica, G. Pilet, G. Chastanet, W. Wernsdorfer, J.-F. Jacquot, D. Luneau *Ange. Chem. Int. Ed.* 2006, **45**, 4659-4662

[22] a) K. Katoh, Y. Horii, N. Yasuda, W. Wernsdorfer, K. Toriumi, B. K. Breedlove and M. Yamashita, *Dalton Trans.*, 2012, **41**, 13582; b) A. Watanabe, A. Yamashita, M. Nakano, T. Yamamura and T. Kajiwara, *Chem. Eur. J.*, 2011, **17**, 7428; c) P.-E. Car, M. Perfetti, M. Mannini, A. Favre, A. Caneschi and R Sessoli, *Chem. Commun.*, 2011, **47**, 3751.

[23] a) G. Abbas, Y. Lan, G. E. Kostakis, W. Wernsdorfer, C. E. Anson, A. K. Powell *Inorg. Chem.* 2010, **49**, 8067; b) S. K. Langley, N. F. Chilton, I. A. Gass, B. Moubaraki, K. S. Murray *Dalton. Trans.* 2011, **40**, 12656.